Monoclinic B-phase erbium sesquioxide (Er_2O_3) thin films by filtered cathodic arc deposition

Christoph Adelhelm[1*], Thomas Pickert[1], Martin Balden[1], Marcin Rasinski[1,2], Tomasz Plocinski[2], Carlos Ziebert[3], Freimut Koch[1*] and Hans Maier[1]

[1]Max-Planck-Institut für Plasmaphysik, Materials Research, EURATOM Association, Boltzmannstraße 2, 85748 Garching, Germany

[2]Faculty of Materials Science and Engineering, Warsaw University of Technology, ul. Wołoska 141, 02-507 Warsaw, Poland

[3]Forschungszentrum Karlsruhe, Institute for Materials Research I, Hermann-von-Helmholtz-Platz 1, 76344 Eggenstein-Leopoldshafen, Germany

Abstract

Er_2O_3 sesquioxide thin films in the uncommon, monoclinic phase were produced for the first time by filtered cathodic arc deposition on Eurofer steel substrates. This was achieved by applying a sample bias of -250 V and deposition temperatures ≤400 °C. XRD texture analysis revealed a strong preferred orientation of the B-phase crystallites. Deposition at 600 °C without bias voltage resulted in thin films showing the regular cubic phase. A dense, columnar structure was found for both phases by scanning transmission electron microscopy.

* Corresponding authors: C. Adelhelm (christoph.adelhelm@ipp.mpg.de), F. Koch (freimut.koch@ipp.mpg.de).

Introduction

Thin films of erbium oxide Er_2O_3 have been investigated with respect to different application fields in the last years. Due to the high dielectric constant (≈14) it is a candidate material to replace the gate dielectric SiO_2 in the next generation of complementary metal oxide semiconductor devices (CMOS) with an oxide layer thickness below 2 nm [1, 2]. Recent research also comprised optoelectronic applications [3, 4] and antireflective coatings [5]. For nuclear fusion applications Er_2O_3 coatings are currently investigated as effective hydrogen diffusion barrier [6, 7] and corrosion resistant, electrically insulating layers [8]. For these applications resistance against radiation damage is of importance.

The polymorphism of rare earth sesquioxides RE_2O_3 is well known [9, 10], and temperature or pressure-induced phase transformations of RE_2O_3 bulk materials have been intensively studied. Generally, five polymorphs are reported, but only three phases (C, H, B) have been observed for Er_2O_3. The cubic C-phase is the stable phase below 2600 K and is usually formed during preparation of Er_2O_3 coatings, even if some authors report about unidentified peaks in x-ray diffractograms [7, 11, 12]. Above 2600 K the hexagonal H-phase occurs. Hoekstra and Gingerich [13] published first about the pressure-induced C- to B-phase transformation at high temperature. Recently this was achieved at room temperature [14], and the B-phase could be quenched to ambient conditions. Lopato et al. [15] proposed the formation of the monoclinic B-phase during high-temperature DTA measurements. Very recently, Guo et al. [16] prepared monoclinic Er_2O_3 nanoparticles by a flame synthesis process at atmospheric pressure. In this letter we report about the preparation of monoclinic B-phase Er_2O_3 thin films for the first time.

Experimental

A magnetically filtered cathodic arc device [17] was used for film deposition. The filter prevents molten erbium droplets from reaching the substrate, which ensures a high coating quality at high deposition rates. Pure erbium (99.9 %) was used as cathode material. After evacuation to a base pressure of about $3x10^{-3}$ Pa the polished Eurofer steel [18] substrates (20 mm in diameter) were etched by an Ar RF plasma. During film deposition, the arc current was about 80 A and 25 sccm oxygen were introduced by a capillary near the substrate resulting in a pressure of $7x10^{-2}$ Pa. A negative RF bias voltage can be applied to the substrate in order to accelerate the Er ions to the substrate. Substrate heating was achieved by means of a BN heater in the sample holder, and the temperature was controlled by an IR-pyrometer. The deposition time was 15 minutes for all samples.

Grazing incidence x-ray diffraction (XRD) in parallel beam geometry was used for phase analysis (θ-scans). In addition, θ scans under different tilt angles were performed for texture analysis. A graphite monochromator was used on the secondary side to reduce the fluorescence background from the substrate. Since no reference spectrum of the monoclinic B-phase was available in any database, we calculated a diffraction pattern using the program PowderCell [19]. The measured lattice parameters and calculated atom positions published by Guo et al. [14] were used as input parameters. A focused ion beam microscope (FIB) was used for the preparation of STEM lamellas as well as argon ion milling in a Gentle Mill device for final thinning and elimination of FIB defects. STEM observation was carried out on a 200 kV UHR STEM microscope (Hitachi HD-2700) equipped with a C_s corrector. A 2.5 MeV H^+ beam was used for the determination of the atomic film composition by Rutherford backscattering spectroscopy (RBS). As mechanical properties the nanohardness H and the reduced Young's modulus E* were measured on a CSIRO UMIS2000 nanoindentation

system at a maximum load of 2 mN, i.e. ≈50 nm indentation depth. For each sample nine load-displacement curves were evaluated using the software IndentAnalyser [20].

Results

Depending on sample bias voltage and deposition temperature, the Er_2O_3 films show different crystallinity. In Fig. 1 diffractograms of Er_2O_3 films on Eurofer substrates are shown using three different deposition conditions. For comparison, two calculated reference patterns of B- and C-phase are also given. At a sample temperature of 600 °C without additional bias the cubic C-phase can be observed (Fig. 1 a). The relative peak intensities are similar to the calculated diffraction pattern, which indicates a mainly texture-free thin film. Deposition temperatures ≤ 400 °C leads to significant deviations from the C-phase reference pattern.

A different Er_2O_3 crystalline structure can be observed by applying a sample bias. Datasets b and c in Fig. 1 show XRD patterns for depositions at RT and 400 °C with -250 V bias voltage. RBS analysis on Er_2O_3 films grown on graphite substrate confirmed the Er_2O_3 stoichiometry for these deposition conditions. The crystal structure can be assigned to the high-pressure, monoclinic B-phase. However, a strong preferred orientation is responsible for missing peaks compared to the simulated standard spectrum (e.g. at 29° and 33°). This is demonstrated in Fig. 2, where diffraction patterns of the B-phase sample from Fig. 1c (400 °C, -250 V) between 2θ=26-35° are presented as a function of the tilt angle χ. After tilting by 30° the (111) peak is visible, for 40° and higher the (-112) peak occurs. Other missing peaks at higher scattering angles (e.g. (313) at 2θ=48.5°) could also be detected by this method. Despite different intensities of the diffraction peaks, no significant difference of the diffraction patterns could be observed for both B-phase thin films deposited at RT or 400 °C.

The microstructure of the C- and B-phase Er_2O_3 thin films was investigated by STEM and micrographs of two cross sections are shown in Fig. 3. Both Er_2O_3 films exhibit a dense structure without voids. The C-phase thin film (Fig. 3a) grows in columns with a maximum

diameter of 100-200 nm. A nucleation zone in the first 100 to 200 nm can be observed, after that zone the columns grow mainly undisturbed. The B-phase film also shows columnar growth, but with smaller columns (50-100 nm), and the growth appears to be more disturbed (Fig. 3b).

The mechanical properties of C and B-phase films are comparable, as determined by nanoindentation. The C-phase coating showed a nanohardness H of 24 ± 1 GPa and a reduced Youngs modulus E* of 308 ± 20 GPa. For the B-phase film (400 °C, -250 V) H was determined to be 20 ± 2 GPa and E* to be 264 ± 7 GPa.

The B-phase is metastable at ambient conditions and can transform into the C-phase at elevated temperatures. In Fig. 4 the XRD patterns of both B-phase thin films are presented before and after annealing to 600 °C for 2 h in vacuum. Annealing does not lead to a phase transformation in the case of a deposition temperature of 400 °C (Fig. 4, top), only variations in peak intensities can be observed. However, the coating deposited at RT (Fig. 4, bottom) transformed into the cubic phase after annealing. Even though the cubic phase has about 8 % lower crystallographic density, the coating remained intact after the phase transformation, and no delamination was observed.

Discussion

The formation of the B-phase during the thin film growth by cathodic arc deposition could in principle be explained by two effects. First, due to the applied bias voltage, the erbium ions are accelerated to the substrate, leading to an intense ion bombardment in the top 1-2 nm during film growth. It has been shown by Tang et al. [21] that irradiation damage produced by ion bombardment (300 keV Kr^{2+}) leads to a C to B phase transformation. Even if the ion energy was much higher in these experiments, Er bombardment of the growing Er_2O_3 film could also explain the formation of the monoclinic phase. The low deposition temperature and

a high deposition rate (≈0.8 nm/s) could lead to quenching of the B-phase, due to sufficiently low atom mobility. This is supported by the fact that by increasing the deposition temperature from 400 °C to 600 °C (at -250 V bias) x-ray diffraction indicated the formation of both phases. The second explanation for the formation of a B-phase thin film is based on the fact that the B-phase forms under high pressure [13, 14]. Guo et al. [16] explained the formation of the B-phase by the high surface tension during formation of Er_2O_3 nanoparticles, resulting in a high internal pressure during particle formation. We also suggest that the XRD patterns of Er_2O_3 coatings published by Jankowski et al. [11] could be explained by the formation of the B-phase at temperatures ≤580 °C. They grew the films with low energetic species by electron beam evaporation of Er_2O_3. B-phase formation could be explained by a high compressive stress during film growth. The influence of compressive stress as a result of the bias voltage could also be responsible for the B-phase formation of our films. Since the deposition temperature influences the stress state of the film, this could explain the different phase stability of the B-phase films for annealing to 600 °C (Fig. 4). Annealing of the sample deposited at room temperature leads to transformation into the C-phase, whereas the sample deposited at 400 °C remained stable. The higher thermal stress occurring in the RT deposited sample during annealing could explain the phase transformation. However, the thermal expansion coefficient of the B-phase needs to be known to prove this explanation; but the thermal expansion properties are unknown up to now.

In this letter we showed for the first time the preparation of Er_2O_3 thin films in the uncommon monoclinic B-phase by filtered cathodic arc deposition. A new Er_2O_3 modification is not only interesting for catalytic or optical applications, but also for nuclear fusion applications. As already discussed, it was recently shown that ion-induced displacement damage of the Er_2O_3 C-phase leads to transformation into the B-phase in the implantation zone [21]. It could be speculated that the performance of a hydrogen diffusion barrier coating or electrical insulating coating is affected by this process. The B-phase could be much more stable against intense

neutron displacement damage occurring in a fusion power reactor, because it is formed under irradiation. Starting already with a B-phase coating could possibly improve the long-term stability. Further experiments are in progress to investigate the influence of film stress on the B-phase formation and its temperature stability. The resistance of the B-phase against ion-induced radiation damage will be investigated and compared to the C-phase.

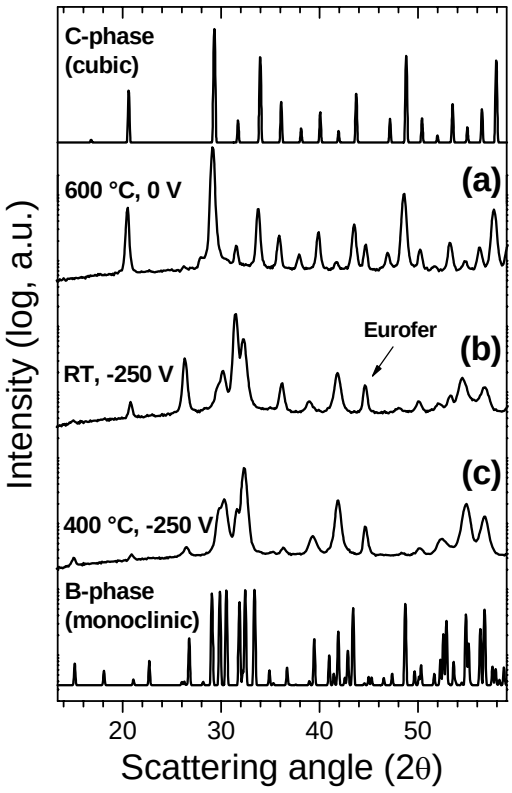

Fig. 1: X-ray diffraction patterns of Er_2O_3 thin films at different deposition conditions (θ-scans at a fixed incident angle of 3°). The cubic C-phase is formed at a deposition temperature of 600 °C without bias (a). The monoclinic phase B-phase is observed for coatings deposited with -250 V bias voltage at (b) RT and (c) 400 °C. Calculated XRD patterns are given at the top (C-phase) and bottom (B-phase). A diffraction peak resulting from the Eurofer steel substrate is observed in all spectra and indicated by an arrow.

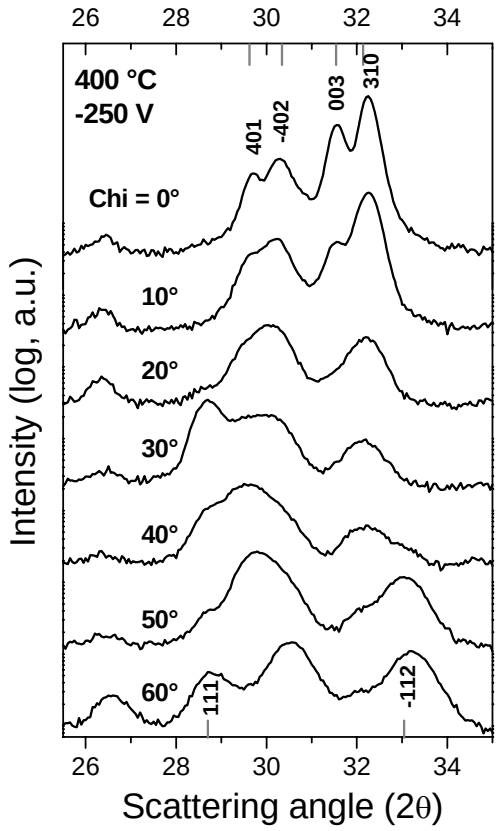

Fig. 2:

X-ray diffractograms (θ-scans, ω=17°) of the B-phase Er_2O_3 thin film deposited at 400 °C and -250 V bias at different tilt angles χ. The indices of the diffraction peaks are indicated. Their positions are shifted by 0.3 to lower 2θ compared to the calculated values.

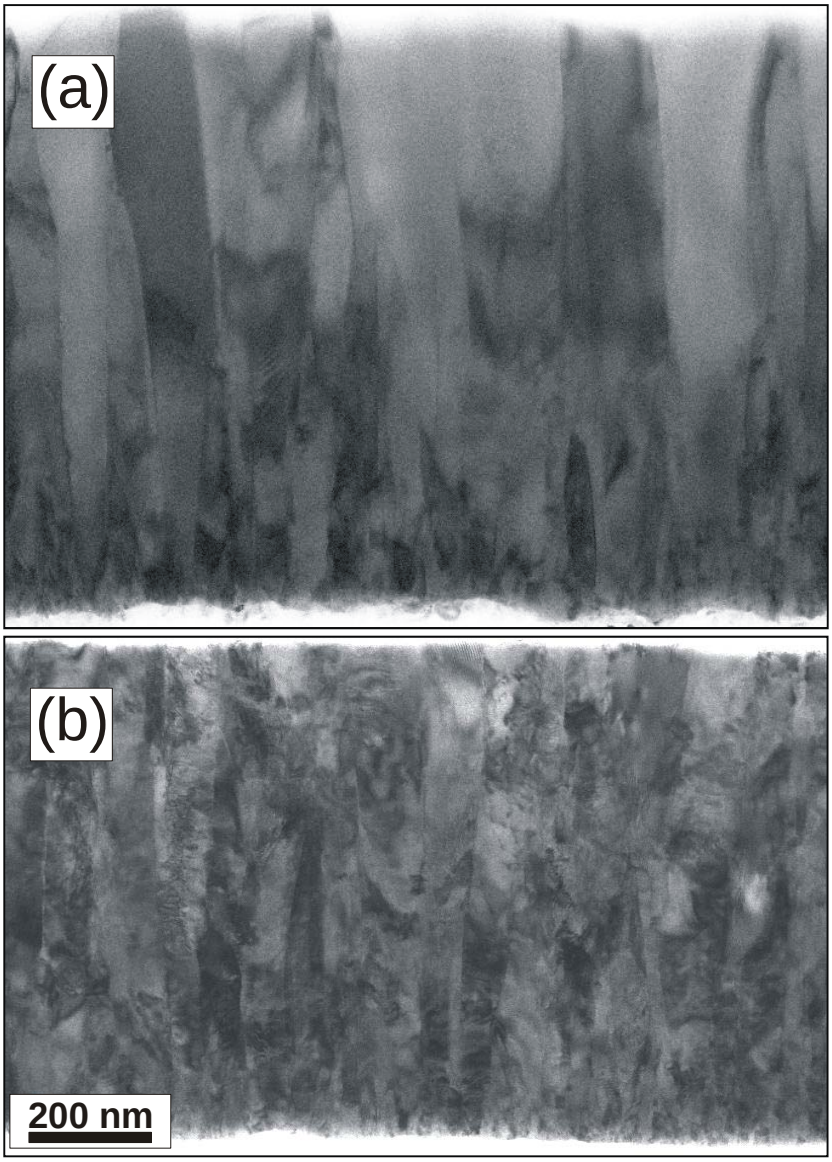

Fig. 3:

STEM cross sections of thin lamellas of Er_2O_3 thin films. (a) cubic C-phase deposited at 600 °C, no bias; (b) monoclinic B-phase deposited at 400 °C with -250 V bias. The contrast was optimized for the film microstructure; therefore the Eurofer substrate and the FIB tungsten top coating appear white.

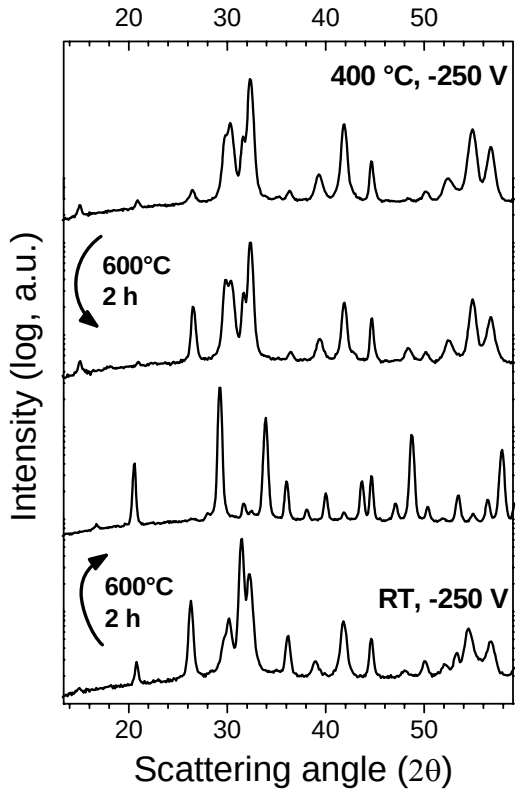

Fig. 4:

X-ray patterns (θ-scans) of B-phase Er_2O_3 thin films before and after annealing to 600 °C in vacuum, showing the influence of deposition temperature on the phase stability. The sample deposited at RT (bottom) transforms into the C-phase, whereas the sample deposited at 400 °C (top) shows no phase transformation.

[1] M. Losurdo, M.M. Giangregorio, G. Bruno, D. Yang, E.A. Irene, A.A. Suvorova, M. Saunders, Appl. Phys. Lett. 91 (2007) 091914.
[2] S. Chen, Y.Y. Zhu, R. Xu, Y.Q. Wu, X.J. Yang, Y.L. Fan, F. Lu, Z.M. Jiang, J. Zou, Appl. Phys. Lett. 88 (2006) 222902.
[3] M. Miritello, R. Lo Savio, A.M. Piro, G. Franzo, F. Priolo, F. Iacona, C. Bongiorno, Journal of Applied Physics 100 (2006) 013502.
[4] C.P. Michael, V.A. Sabnis, H.B. Yuen, A. Jamora, S. Semans, P.B. Atanackovic, O. Painter, Appl. Phys. Lett. 94 (2009) 131103.
[5] M. Losurdo, M.M. Giangregorio, P. Capezzuto, G. Bruno, R.G. Toro, G. Malandrino, I.L. Fragala, L. Armelao, D. Barreca, E. Tondello, A.A. Suvorova, D. Yang, E.A. Irene, Adv. Funct. Mater. 17 (2007) 3607.
[6] D. Levchuk, S. Levchuk, H. Maier, H. Bolt, A. Suzuki, J. Nucl. Mater. 367 (2007) 1033.
[7] F. Koch, R. Brill, H. Maier, D. Levchuk, A. Suzuki, T. Muroga, H. Bolt, J. Nucl. Mater. 329-33 (2004) 1403.
[8] T. Muroga, J.M. Chen, V.M. Chernov, K. Fukumoto, D.T. Hoelzer, R.J. Kurtz, T. Nagasaka, B.A. Pint, M. Satou, A. Suzuki, H. Watanabe, J. Nucl. Mater. 367 (2007) 780.
[9] L. Eyring. Chapter 27, The binary rare earth oxides In: K.A. Gschneidner Jr, L. Eyring, editors. Handbook on the Physics and Chemistry of Rare Earths, vol. 3. North-Holland Publishing Company, 1979. p.337.
[10] G. Adachi, N. Imanaka, Z.C. Kang. Binary Rare Earth Oxides. Dordrecht, The Netherlands: Kluwer Academic Publishers, 2004.
[11] A.F. Jankowski, C.K. Saw, J.L. Ferreira, J.S. Harper, J.P. Hayes, B.A. Pint, J. Mater. Sci. 42 (2007) 5722.
[12] A. Sawada, A. Suzuki, H. Maier, F. Koch, T. Terai, T. Muroga, Fusion Engineering and Design 75-79 (2005) 737.
[13] H.R. Hoekstra, K.A. Gingerich, Science 146 (1964) 1163.
[14] Q.X. Guo, Y.S. Zhao, C. Jiang, W.L. Mao, Z.W. Wang, J.Z. Zhang, Y.J. Wang, Inorg. Chem. 46 (2007) 6164.
[15] L.M. Lopato, A.V. Shevchenko, A.E. Kushchevskii, S.G. Tresvyatskii, Inorganic Materials 10 (1974) 1276.
[16] B. Guo, Z.S. Harvey, J. Neil, I.M. Kennedy, A. Navrotsky, S.H. Risbud, J. Am. Ceram. Soc. 90 (2007) 3683.
[17] Y. Yamada-Takamura, F. Koch, H. Maier, H. Bolt, Surface and Coatings Technology 142-144 (2001) 260.
[18] R. Lindau, M. Schirra, Fusion Engineering and Design 58-9 (2001) 781.
[19] PowderCell. http://www.bam.de/de/service/publikationen/powder_cell.htm.
[20] www.asmec.de. IndentAnalyser.
[21] M. Tang, P. Lu, J.A. Valdez, K.E. Sickafus, Journal of Applied Physics 99 (2006) 063514.